JOURNAL OF GUIDANCE, CONTROL, AND DYNAMICS
Vol. 16, No. 6, November–December 1993

# $H_\infty$ Optimized Wave-Absorbing Control: Analytical and Experimental Results

Khoichi Matsuda and Hironori Fujii
*Tokyo Metropolitan Institute of Technology, Hino, Tokyo 191, Japan*

**The wave-absorbing control is a control concept to absorb waves traveling in a flexible structure at actuator positions. This paper presents an approach to design a broadband compensator by applying the $H_\infty$ control theory to the wave-absorbing control method. This approach aims to minimize effects of the incoming waves on the outgoing waves at the actuator positions in the sense that the $H_\infty$ norm of the closed-loop scattering matrix is minimum. Vibration suppression control for a flexible beam is studied analytically and demonstrated experimentally to exemplify the controller design approach. Compensators are designed for a collocated torque actuator and angle sensor and also for a noncollocated torque actuator and bending moment sensor. Performance of the compensators is analyzed in the frequency domain, and measured open- and closed-loop transfer functions are obtained from random excitation tests. The designed compensators are shown to attain good broadband damping, and results of the experiments are shown to agree well for the range of frequency below 50 Hz with those of the numerical simulations.**

## I. Introduction

ACTIVE control of vibrations in large flexible structures has received considerable attention in recent years. The modal model is a powerful technique both for the dynamic analysis and for the control design. However, limitations on the applicability of the structural modal analysis exist[1] when the requirements for vibration suppression and pointing accuracy for flexible structures become stringent. The flexible mode frequencies and shapes are extremely sensitive to inevitable modeling errors, and modal analysis cannot provide a sufficiently accurate design model over a modally rich frequency range.

One alternative is the traveling wave approach. This approach is based on the property that the response of a flexible structure to a typical locally applied force can be viewed in terms of traveling elastic disturbances. Mathematically, traveling waves belong to homogeneous solutions of partial differential equations describing the vibration of continua. At controller positions, relations between incoming and outgoing wave vectors and control inputs are derived in a matrix form by representing boundary conditions in terms of the traveling wave vectors. Outgoing waves are produced by the reflection of the incoming waves and are generated by control inputs. Transfer functions from the incoming wave and control input vectors to the outgoing wave vector are called scattering and generating matrices, respectively. Control inputs are set to be in the output-feedback form. This leads to the closed-loop relations between outgoing and incoming waves. Compensators are selected so that the effects of the incoming waves on the outgoing waves are reduced in some sense by adequately selecting elements of the closed-loop scattering matrix. Characteristic elements of the wave-propagation model, such as a scattering matrix, are smooth functions with respect to frequency and are more insensitive to model uncertainties than mode frequencies and shapes. The approach can provide a sufficiently accurate model for a controller design over a modally dense frequency region, and considerable research has been done on the wave control methods.[1-8] However these methods also have drawbacks, such as 1) the designed compensator is not guaranteed to be a causal and real function with

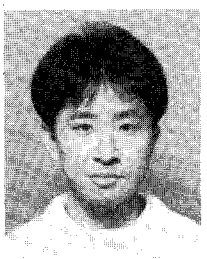

**Khoichi Matsuda was born in Saitama, Japan, on March 13, 1969. He received the B.E. and M.E. degrees in aerospace engineering in 1991 and 1993, respectively, from the Tokyo Metropolitan Institute of Technology. He is currently a graduate student in the doctoral program of the Tokyo Metropolitan Institute of Technology. His research interests include dynamics and control of large space structures. He is a Student Member of AIAA and the Japan Society for Aeronautical and Space Sciences.**

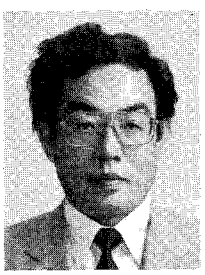

**Hironori Fujii is a professor in the Department of Aerospace Engineering and a chairman for graduate studies at the Tokyo Metropolitan Institute of Technology. He earned his D.E. degree in 1975 from Kyoto University. His research interests include dynamics and control of large space structures and robotics for aerospace application. Since 1982 he has been responsible for the coordination of the Research Group on Control of Flexible Space Structures in Japan. He is a Member of AIAA, the American Astronautical Society, and the Japan Society for Aeronautical and Space Sciences, and he is an Associate Fellow of the Canadian Aeronautics and Space Institute.**

Received June 25, 1992; revision received March 20, 1993; accepted for publication March 20, 1993. 

respect to the Laplace variable, 2) the closed-loop system is not guaranteed to be stable, and 3) these methods are only applicable to such a simple structure as networks of waveguides. From a similar viewpoint, MacMartin and Hall[9,10] have recently shown a more general technique using the dereverberated driving point mobility of structure. This control law minimizes the maximum value of the power flow entering the structure, resulting in power dissipation over all frequency ranges. This technique does not have all of the drawbacks stated earlier, although a single-input/single-output system with a collocated rate sensor must be assumed.

This paper presents an approach for designing a broadband compensator by applying the $H_\infty$ control theory to the wave-absorbing control method. This approach aims to minimize effects of the incoming waves on the outgoing waves at the actuator positions in the sense that the $H_\infty$ norm of the closed-loop scattering matrix is minimum. This can be interpreted as minimizing the worst case $H_2$ norm of the reflection waves, and the designed compensator is guaranteed to be a real and causal function. The limitations are that the closed-loop system is not proved to be stable and that the method is not applicable to general structures that cannot be described by partial differential equations. However, this approach can use various sensors that may be noncollocated at actuators and may be applied to a multi-input/multi-output system. This is a favorable feature for implementing the controllers from a practical point of view. Damping performance of a closed-loop system is improved by employing noncollocated sensors and actuators at the sacrifice of the stability margin in many cases. The goal is to construct a reliable control technique for a multi-input/multi-output system with noncollocated sensor/actuator pairs. Large space structures currently suggested have such rather simple shapes as whole behaviors are well described by partial differential equations. The present approach is applied for an example to designing compensators for vibration suppression of a hanging pinned-free beam. Compensators are designed for a collocated torque actuator and angle sensor and also for a noncollocated torque actuator and bending moment sensor. The performance of the compensators is analyzed in the frequency domain. Results of the hardware experiments are also reported for verifying validity of the presented technique. Measured open- and closed-loop transfer functions are obtained through random excitation tests. The designed compensators attain broadband damping, and good agreement is shown between the measured and calculated closed-loop transfer functions for the frequency range below 50 Hz.

## II. Controller Design

Various disturbance waves are generated at certain points in a large flexible structure and propagate through the structure. The disturbance waves will be scattered at actuators, which are located at junctions or discontinuities. The technique presented here aims to minimize effects of the incoming waves on the outgoing waves at actuator positions in an $H_\infty$ sense. Specifically, the technique minimizes the $H_\infty$ norm of the closed-loop transfer function from the incoming waves to the outgoing waves, i.e., the scattering matrix. From the definition of the $H_\infty$ norm, it can be interpreted as a technique that minimizes the worst-case amplitudes of the outgoing disturbances. The problem is formulated as a four-block problem that affords a systematic technique to obtain the solutions in the $H_\infty$ control theory.

Suppose a flexible structure consists of several slender structural members that are well described by partial differential equations. Applying Laplace transformation to these equations and boundary conditions at controller positions, one can derive causal relations between incoming and outgoing waves, sensor outputs $y$, and controller inputs $u$ as follows:

$$b = Sa + Bu \tag{1}$$

$$y = Ta + Gu \tag{2}$$

where $a$ is the incoming waves into the sensor positions, $b$ the outgoing waves from the actuator positions, $S$ the scattering matrix whose entries are reflection coefficients, and $G$ the transfer function of the "infinitely extended" system such as a semi-infinite beam.[9,10] Equations (1) and (2) can be written in the following form:

$$\left[\begin{array}{c} b \\ \hline y \end{array}\right] = \left[\begin{array}{c|c} S & B \\ \hline T & G \end{array}\right] \left[\begin{array}{c} a \\ \hline u \end{array}\right] \tag{3}$$

In the present analysis the controller inputs are limited to the form

$$u = Ky \tag{4}$$

where $K$ is a compensator. Equations (2) and (4) give the control in terms of the incoming waves as follows:

$$u = K(I - GK)^{-1}Ta \tag{5}$$

$$= HTa \tag{6}$$

where $I$ is an identity matrix. From Eqs. (5) and (6), $K$ is related to $H$ via

$$K = H(I + HG)^{-1} \tag{7}$$

Substituting Eq. (6) into Eq. (1) gives the following closed-loop relation between $a$ and $b$:

$$b = (S + BHT)a \tag{8}$$

$$= S_{cl}a \tag{9}$$

where $S_{cl}$ is the closed-loop scattering matrix. Then the problem is to find a causal compensator $K$ that minimizes the worst-case amplitudes of the outgoing waves. On making use of the relation between the $H_\infty$ norm and the $H_2$ norm,[11] we obtain

$$\|S_{cl}\|_\infty = \sup\left(\frac{\|b\|_2}{\|a\|_2} : a \in H_2\right) \tag{10}$$

where $a$ is assumed to be in $H_2$. A compensator $K$ that minimizes $\|S_{cl}\|_\infty$ is then selected to our end.

This problem can be regarded as a four-block problem in the $H_\infty$ control theory[11-13] if the controlled output vector is chosen to be an outgoing wave vector $b$. If control cost is added to the controlled output vector $z$, Eq. (3) is modified as

$$\left[\begin{array}{c} z \\ \hline y \end{array}\right] = \left[\begin{array}{c|c} W_1S & W_1B \\ 0 & W_2 \\ \hline T & G \end{array}\right] \left[\begin{array}{c} a \\ \hline u \end{array}\right] \tag{11}$$

where $W_1$ and $W_2$ are frequency-weighting functions, $\|z\|_2 = \sqrt{(\|W_1b_2\|)^2 + (\|W_2u_2\|)^2}$, and $\mathbf{0}$ is a null matrix. Usually, model uncertainties become larger for a higher frequency region, and compensators must roll off at a high frequency. Disturbance waves probably occur at a low frequency in flexible structures. Hence $W_1$ and $W_2$ can be chosen to be low-pass and high-pass filters, respectively. This is one of the mixed-sensitivity optimization problems well known in the $H_\infty$ control theory.

Four-block problems, as shown in Eqs. (3) and (11), can be solved numerically in state-space form when it is difficult to find an analytic solution. It should be noted that to apply the state-space formula irrational functions must be suitably approximated over the frequency range of interest; for example, by continued-fraction expansion, Padé approximation, and so on. It is also noted that stability is not yet proved in general for the closed-loop systems with compensators designed by this technique.

## III. Flexible Beam Examples

A vibration suppression for a flexible beam is studied analytically and demonstrated experimentally to exemplify the foregoing controller design approach.

### Experimental Setup

A pinned-free homogeneous flexible beam is chosen as a test structure. The beam (Fig. 1) consists of a stainless sheet of thickness 1.0 mm, width 3.0 cm, and length 2.0 m. The bending rigidity and mass per unit length are 0.52 N·m$^2$ and 0.24 kg/m, respectively. The beam is connected to the shaft of a dc torque motor used as an actuator and supported by a structure fixed to the wall. The sensors consist of strain gauges to measure the bending moment and an angular potentiometer to measure the angle of horizontal deflection at the upper end of the beam. The strain gauges are located at the root of the beam, at 7.5% of the beam length. Nonminimum phase zeros are one of the important characteristics in the noncollocated sensor and actuator system. The location of the strain gauges is a node of the vibration mode at about 100 Hz. These sensor signals are amplified and put into a digital computer (with a 32-bit CPU) through an analog-to-digital converter. The computer outputs a control signal to drive two dc torque motors through a digital-to-analog converter: one is an actuator to suppress the vibration of the beam, and the other is a shaker to provide a disturbance force at the lower end of the beam. The shaker is attached to the beam through a stick with a pinned connection as shown in the Fig. 1. This test structure is modeled mathematically as a pinned-free beam.

### Dynamic Model and Controller Design

A dynamic model of the flexible beam is based on the Euler-Bernoulli theory. The partial differential equation governing the dynamics of the beam with the gravitational force $S(x)=\rho A g(L-x)$ is written in the form:

$$EI\frac{\partial^4 v}{\partial x^4}-\frac{\partial}{\partial x}\left(S\frac{\partial v}{\partial x}\right)+\rho A\alpha\frac{\partial v}{\partial t}-EI\beta\frac{\partial^3 v}{\partial t\,\partial x^2}+\rho A\frac{\partial^2 v}{\partial t^2}=0 \tag{12}$$

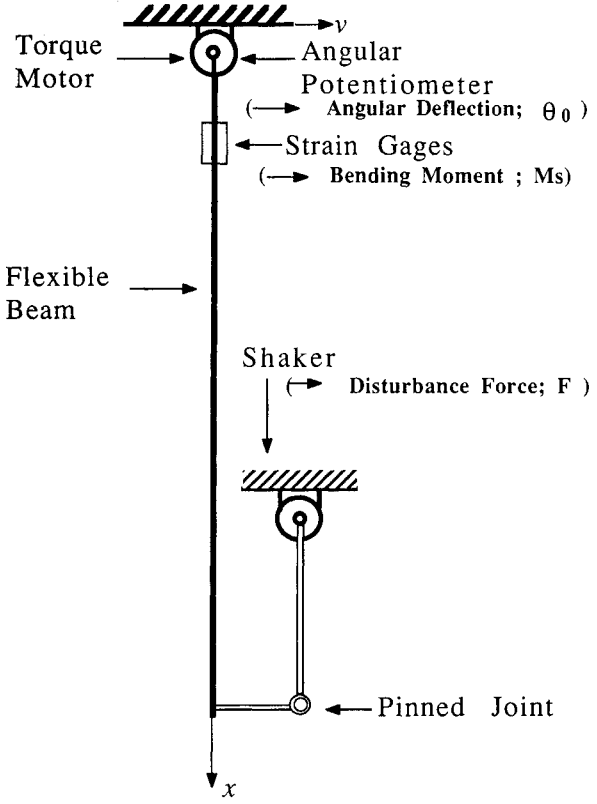


**Fig. 1 Flexible beam test setup.**

together with the boundary conditions

$$v(0,t)=0,\qquad EI\frac{\partial^2 v}{\partial x^2}(L,t)=0$$
$$EI\frac{\partial^2 v}{\partial x^2}(0,t)=M_c,\qquad EI\frac{\partial^3 v}{\partial x^3}(L,t)=0 \tag{13}$$

where $v(x,t)$ is the lateral displacement, $EI$ the bending rigidity, $\rho A$ the mass per unit length, $L$ the beam length, and $M_c$ the applied control torque. Damping effects are included as shown in Eq. (12). The third and fourth terms on the left-hand side of Eq. (12) are viscous and Chen-Russel damping, respectively.[14] Equations (12) and (13) are employed in system parameter identifications and numerical simulations of the open- and closed-loop performance. The damping and gravitational force terms are ignored in the following controller design for the sake of brevity, and Eq. (12) leads to

$$EI\frac{\partial^4 v}{\partial x^4}+\rho A\frac{\partial^2 v}{\partial t^2}=0 \tag{14}$$

The application of the Laplace transformation, with $s$ as the time transform variable, to Eq. (14) provides the ordinary differential equation (to avoid new symbols, the transformed variables hereafter have the same notation as their time-dependent equivalents)

$$a^2\frac{\mathrm{d}^4 v}{\mathrm{d}x^4}+s^2 v=0 \tag{15}$$

where $a^2=EI/\rho A$. The analysis proceeds with the introduction of the cross-sectional state vector $Y=(v\ \dot\theta\ m\ q)^T$, where $\dot v=sv$ is the lateral velocity, $\dot\theta=s(\mathrm{d}v/\mathrm{d}x)$ is the angular velocity, $m=(a/EI)M$ with $M=EI(\mathrm{d}^2v/\mathrm{d}x^2)$ the internal bending moment, and $q=(a/EI)Q$ with $Q=EI(\mathrm{d}^3v/\mathrm{d}x^3)$ the internal shear force. In terms of the state vector, the transformed Euler-Bernoulli equation can be written in the form

$$\frac{\mathrm{d}Y}{\mathrm{d}x}=\begin{bmatrix}0&1&0&0\\0&0&p&0\\0&0&0&1\\-p&0&0&0\end{bmatrix}Y=AY \tag{16}$$

where $p=s/a$. Since imaginary variables do not appear explicitly, Eq. (16) can be block diagonalized in a real Jordan canonical form by the transformation as follows:

$$Y=\frac{1}{2}\begin{bmatrix}\sqrt{2}p&0&\sqrt{2}p&0\\p^{3/2}&p^{3/2}&-p^{3/2}&p^{3/2}\\0&\sqrt{2}p&0&-\sqrt{2}p\\-p^{3/2}&p^{3/2}&p^{3/2}&p^{3/2}\end{bmatrix}W=UW \tag{17}$$

This transformation may be interrupted as the presentation of the state vector in terms of traveling waves. Each entry of the new cross-sectional state vector $W$ is the amplitude of a traveling wave mode, and the amplitudes of these wave modes vary according to

$$\frac{\mathrm{d}W}{\mathrm{d}x}=\left(\frac{p}{2}\right)^{1/2}\begin{bmatrix}1&1&0&0\\-1&1&0&0\\0&0&-1&1\\0&0&-1&-1\end{bmatrix}W \tag{18}$$

The cross-sectional state vector $W$ has been ordered as $W=(a_1\,a_2\,b_1\,b_2)^T$, where $b_1$ and $b_2$ are the amplitudes of wave

modes outgoing from the pinned end of the beam, and $a_1$ and $a_2$ are the amplitudes of wave modes incoming into the pinned end of the beam. These propagation directions are related to the wave modes at $x=0$ and $L$ by

$$\begin{bmatrix} a_{1p} \\ a_{2p} \\ b_{1f} \\ b_{2f} \end{bmatrix} = \begin{bmatrix} C(Tp) & -S(Tp) & 0 & 0 \\ S(Tp) & C(Tp) & 0 & 0 \\ 0 & 0 & C(Tp) & S(Tp) \\ 0 & 0 & -S(Tp) & C(Tp) \end{bmatrix} \begin{bmatrix} a_{1f} \\ a_{2f} \\ b_{1p} \\ b_{2p} \end{bmatrix} \tag{19}$$

where $C(Tp)=\exp(-\sqrt{Tp})\cos(\sqrt{Tp})$, $S(Tp)=\exp(-\sqrt{Tp})\times\sin(\sqrt{Tp})$, $T=L^2/2$, and the subscripts $p$ and $f$ denote the pinned and free end of the beam, respectively. The elements of the matrix in Eq. (19) are analytic on the right half of the complex Laplace plane and thus are causal.

Compensators are designed for a collocated torque actuator and angle sensor and also for a noncollocated torque actuator and bending moment sensor in the following sections.

#### Collocated Torque Actuator and Angle Sensor

In this case the causal relations are derived between incoming and outgoing waves, a sensor output, and a controller input in the matrix form:

$$\begin{bmatrix} \boldsymbol{b} \\ \hline m_s \end{bmatrix} = \left[\begin{array}{cc|c} -C(tp) & -S(tp) & 0 \\ -S(tp) & C(tp) & -\sqrt{2}p^{-1} \\ \hline \sqrt{2}pC(tp)S(tp) & p[1-C(tp)^2+S(tp)^2]/\sqrt{2} & C(tp) \end{array}\right] \begin{bmatrix} \boldsymbol{a}_s \\ \hline m_c \end{bmatrix} \tag{26}$$

where $t=L_s^2/2$, $L_s$ is a sensor position, and the subscripts $s$ and $c$ denote sensor and controller positions, respectively. This four-block problem can be solved numerically. The designed compensator, however, does not roll off, and instability is caused for a high-frequency region in the experiment. Frequency-weighting functions are thus added to the performance index for the compensator to roll off, and Eq. (26) is modified as follows:

$$\begin{bmatrix} \boldsymbol{z} \\ \hline m_s \end{bmatrix} = \left[\begin{array}{cc|c} -W_1C(tp) & -W_1S(tp) & 0 \\ -W_1S(tp) & W_1C(tp) & -\sqrt{2}W_1p^{-1} \\ 0 & 0 & W_2 \\ \hline \sqrt{2}pC(tp)S(tp) & p[1-C(tp)^2+S(tp)^2]/\sqrt{2} & C(tp) \end{array}\right] \begin{bmatrix} \boldsymbol{a}_s \\ \hline m_c \end{bmatrix} \tag{27}$$

$$\begin{bmatrix} \boldsymbol{b} \\ \hline \dot{\theta} \end{bmatrix} = \left[\begin{array}{cc|c} -1 & 0 & 0 \\ 0 & 1 & -\sqrt{2}p^{-1} \\ \hline p^{3/2} & p^{3/2} & -(p/2)^{1/2} \end{array}\right] \begin{bmatrix} \boldsymbol{a} \\ \hline m_c \end{bmatrix} \tag{20}$$

where $m_c=(a/EI)M_c$. Note that the sensor output is set temporally to be an angular velocity here for the sake of taking the same notations as those of Ref. 2. Modification would be necessary for this case since the sensor output is actually the angle at the pinned end and the controller input is the form

$$m_c = K\dot{\theta} \tag{21}$$

The scattering matrix $\boldsymbol{S}$ is diagonal, the matrix $\boldsymbol{B}$ has a null element in this case, and $\|\boldsymbol{S}_{cl}\|_\infty$ is not adequate to the present case as the performance index since it is more than $\|\boldsymbol{S}\|_\infty=1$ for any controller input. Physically, the reflection waves $b_1$ cannot be modified by the input $u$. Thus the reflection waves $b_2$ are only taken into account, and Eq. (20) is reduced as follows:

$$\begin{bmatrix} b_2 \\ \hline \dot{\theta} \end{bmatrix} = \left[\begin{array}{cc|c} 0 & 1 & -\sqrt{2}p^{-1} \\ \hline p^{3/2} & p^{3/2} & -(p/2)^{1/2} \end{array}\right] \begin{bmatrix} \boldsymbol{a} \\ \hline m_c \end{bmatrix} \tag{22}$$

Equations (8) and (22) give the closed-loop relation between $b_2$ and $\boldsymbol{a}$:

$$b_2 = [-X \quad 1-X]\boldsymbol{a} \tag{23}$$

where $X=\sqrt{2}Hp^{1/2}$. Analytically, as in Ref. 9, the squared largest singular value $\bar{\sigma}^2$ of $[-X \quad 1-X]$ is

$$\bar{\sigma}^2 = 2\left[X(j\omega)-\tfrac{1}{2}\right]\left[X(-j\omega)-\tfrac{1}{2}\right]+\tfrac{1}{2} \tag{24}$$

on the imaginary axis in the complex Laplace plane. Clearly there cannot exist $X(s)$ for which $\|[-X \quad 1-X]\|_\infty<1/\sqrt{2}$. Since the solution $X(s)=\frac{1}{2}$ results in $\|[-X \quad 1-X]\|_\infty=1/\sqrt{2}$, this should be an optimal solution. Therefore, the compensator $C_1(s)$ from $\theta$ to $M_c$ is given by

$$C_1(s) = \frac{\sqrt{2}(EI)^{1/4}(\rho A)^{1/4}\sqrt{s}}{3} \tag{25}$$

This compensator is positive real and causal, and the closed-loop system is guaranteed to be stable. The gain of the compensator so derived is proportional to that of a compensator designed by minimizing the $H_\infty$ norm of the power flow into the structure.[9]

#### Noncollocated Torque Actuator and Bending Moment Sensor

As in the case of the collocated sensor and actuator, relation is derived between incoming and outgoing waves, a sensor output, and a controller input in the matrix form:

where $W_1$ and $W_2$ are frequency-weighting functions. The weighting function $W_1$ consists of two parts, i.e., $W_1=W_{1a}W_{1b}$, where $W_{1a}$ and $W_{1b}$ are chosen to be a high-pass filter to eliminate the rigid-body mode and a low-pass filter to emphasize vibration energy at a low frequency less than 100 Hz, respectively. This is because we aim to achieve a broadband damping rather than a narrow one. The weighting $W_1$ is selected to be a strictly proper second-order filter, and $W_2$ is chosen to be a high-pass filter to emphasize the cost of the control input at high frequency.

The matrix in Eq. (27) has elements of an irrational function. To apply the state-space formula to the four-block problem, these irrational functions are approximated to be a rational polynomial based on the continued-fraction expansion over the frequency range from 0.1 to 100 Hz. (For details see the Appendix.) The approximation of the irrational function $C(tp)$ has a nonminimum phase zero, which is a characteristic of a noncollocated sensor and actuator system. Tuning three parameters of the weighting function and observing a sigma plot of the closed-loop scattering matrix, the second compensator $C_2(s)$ has been designed to be a fifth-order rational polynomial.

For comparison of the damping performance with the designed compensator, the third compensator from $m_s$ to $m_c$ is selected as follows:

$$C_3(s) = \frac{\cos(\alpha\sqrt{s})}{\cosh(\alpha\sqrt{s})} \tag{28}$$

where $\alpha = (\rho A/EI)^{0.25} L_s/\sqrt{2}$. By setting a dominant element of the closed-loop scattering matrix in Ref. 8 to be zero, a compensator is derived as

$$C(s) = \frac{\cos(\alpha\sqrt{s}) - j\sin(\alpha\sqrt{s})}{\cosh(\alpha\sqrt{s})} \tag{29}$$

where $j = \sqrt{-1}$ and a real part of $C(s)$ is the compensator $C_3(s)$. The design of the compensator of Eq. (29) is based on the property that the evanescent wave modes are negligible at high frequency. Since the compensator $C(s)$ is a complex variable with respect to $s$ and only the real part is realizable, the third compensator $C_3(s)$ is selected as Eq. (28).

### Structural Response Simulation

A modal model is employed to numerically simulate the open- and closed-loop structural responses. The eigenfunctions and eigenvalues are calculated by applying Galerkin's method to the partial differential equation, Eq. (12), employing gravity-free pinned-free beam eigenfunctions as trial functions. The eigenfunctions and eigenvalues are calculated in this manner through the use of 20 trial functions, and the first 20 structural modes are employed in the structural response simulation. The modal damping without control is estimated in a semiquantitative fashion: viscous damping factor $\alpha$ and Chen-Russel damping factor $\beta$ are adjusted iteratively until reasonable agreement in resonance peak magnitudes is achieved between measurements and calculations. The damping factors $\alpha$ and $\beta$ are selected to be 0.3 and 0.01, respectively.

The transfer functions from the tip force to the angular deflection at the root of the beam are obtained using the collocated $H_\infty$ compensator $C_1(s)$. Figure 2 compares the open- and closed-loop transfer functions. This compensator causes the damping to be independent of frequency and broadband. This feature is seen to be same as the unweighted $H_\infty$ compensator in Ref. 9.

Figure 3 compares the open- and closed-loop transfer functions using the compensator $C_2(s)$ from the tip force to the bending moment at the root of the beam, at 7.5% of the beam length. Broadband damping is achieved, although the damping magnitude is small due to gravity at the low-frequency region.

Figure 4 compares the same transfer functions as in Fig. 3 in the open- and closed-loop cases using $C_3(s)$. This compensator results in good damping at high frequencies. However, it excites larger deflection than the open-loop case at low frequencies. This effect happens because the evanescent wave modes are not negligible at the low-frequency region.

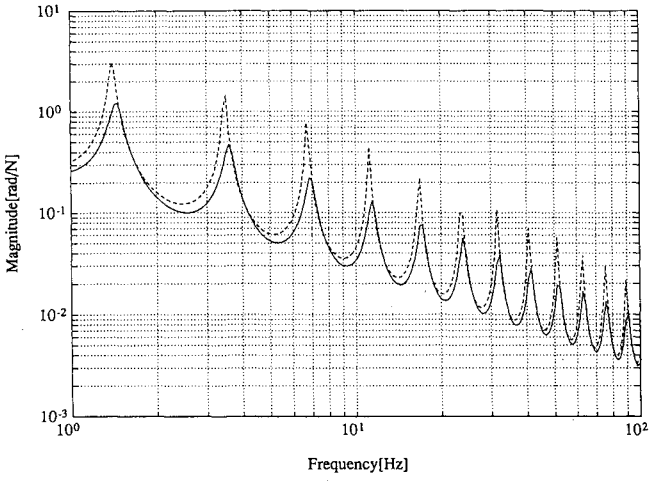


**Fig. 2 Simulated open- (broken) and closed-loop (solid) transfer functions ($\theta_0/F$) using the compensator $C_1(s)$.**

### Experimental Results

The open- and closed-loop transfer functions are employed to verify the performance of the designed compensators. The transfer functions are measured for a frequency range of 1–100 Hz. The $M$-sequence signal (maximum length null sequence) known as a pseudorandom signal is used to excite the system. The $M$-sequence signal employed in this experiment keeps its power spectral density constant up to 100 Hz. The measured transfer functions are calculated from the autoregressive model based on the data of the random excitation tests.

The compensators $C_1(s)$ and $C_3(s)$ are irrational functions and must be approximated to be a rational polynomial. An approximation method is selected to retain only the first several terms in the continued-fraction expansions of the irrational functions. In the case of the compensator $C_1(s)$ the squared magnitudes are approximated on the $j\omega$ axis, which is important for the control system design. At the approximation of the compensator $C_3(s)$, however, the magnitude is constant on the imaginary axis. The singularity is encountered at the continued-fraction expansion in the same manner as the compensator $C_1(s)$. The compensator is thus approximated in this

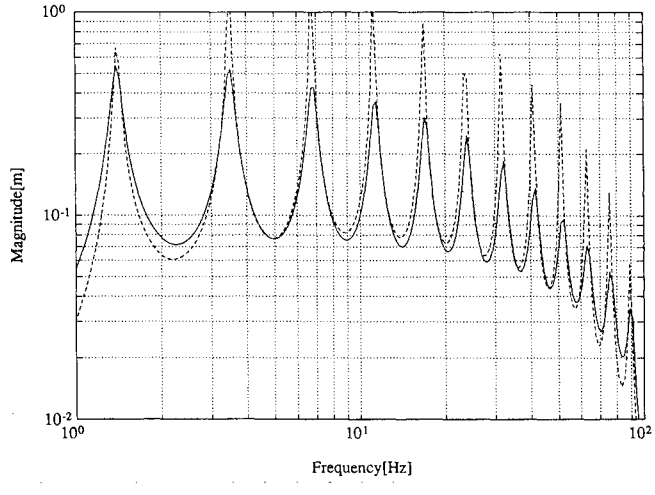


**Fig. 3 Simulated open- (broken) and closed-loop (solid) transfer functions ($M_s/F$) using the compensator $C_2(s)$.**

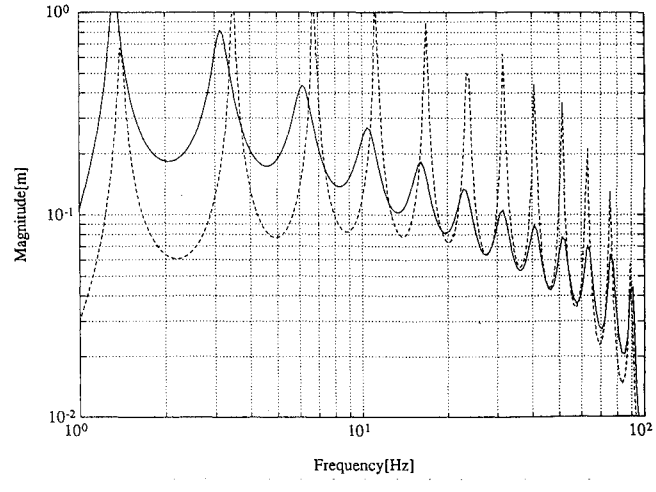


**Fig. 4 Simulated open- (broken) and closed-loop (solid) transfer functions ($M_s/F$) using the compensator $C_3(s)$.**

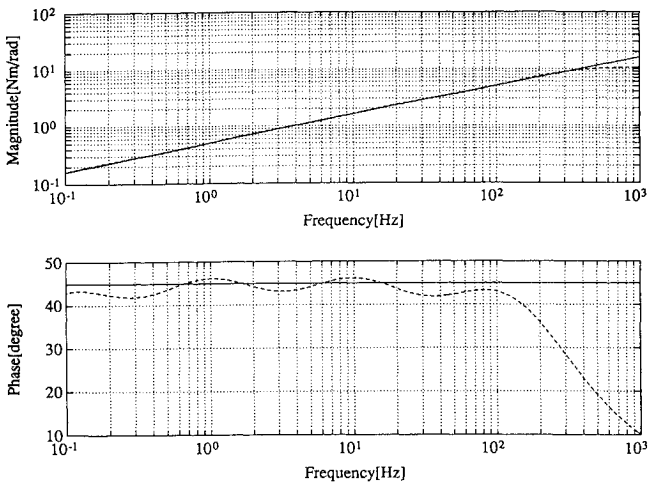


**Fig. 5 Approximated (broken) and desired (solid) transfer functions of the compensator $C_1(s)$.**

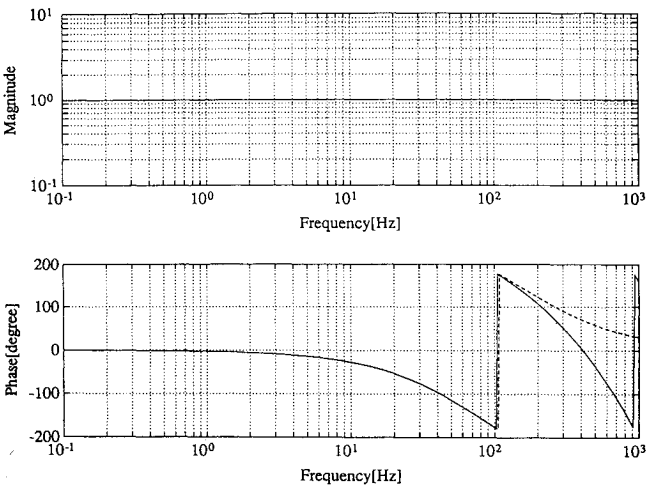


**Fig. 6 Approximated (broken) and desired (solid) transfer functions of the compensator $C_3(s)$.**

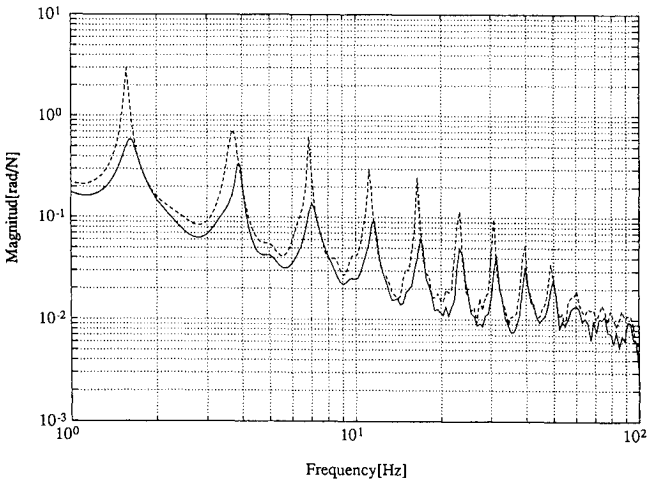


**Fig. 7 Measured open- (broken) and closed-loop (solid) transfer functions ($\theta_0/F$) using the compensator $C_1(s)$.**

case through the use of values on the real axis. The compensators $C_1(s)$ and $C_3(s)$ are approximated to be a fourth- and second-order proper rational polynomial, respectively. The transfer function of the approximated compensator is compared with the ideal $C_1(s)$ in Fig. 5. The magnitude of the ideal compensator is well approximated. The phase deviates by as much as 3 deg from the ideal value in the range from 0.1 to 100 Hz. Figure 6 compares the transfer functions of the desired compensator $C_3(s)$ and the approximation. The transfer function of the desired compensator is successfully approximated, within 0.2 deg of phase, up to a frequency of 100 Hz. In addition to these approximations, all of the compensators are discretized using a Tustin transformation with a sample rate of 1 kHz. The digital filter is implemented by a cascade form in the experiments. Double-precision operations are used to prevent roundoff errors in the control algorithm.

Figure 7 compares the measured transfer functions in the open loop and closed loop using the collocated $H_\infty$ compensator $C_1(s)$. In comparison with the results of Fig. 2, this result shows good agreement between the calculated and measured transfer functions except at the frequency range higher than 50

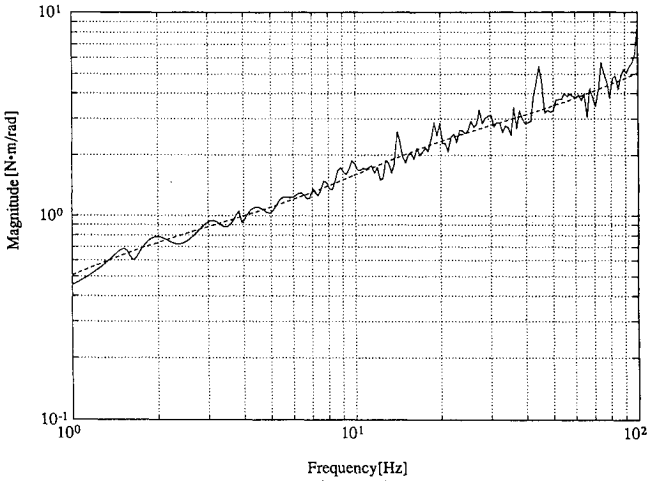


**Fig. 8 Desired (broken) and measured (solid) magnitudes of the compensator $C_1(s)$.**

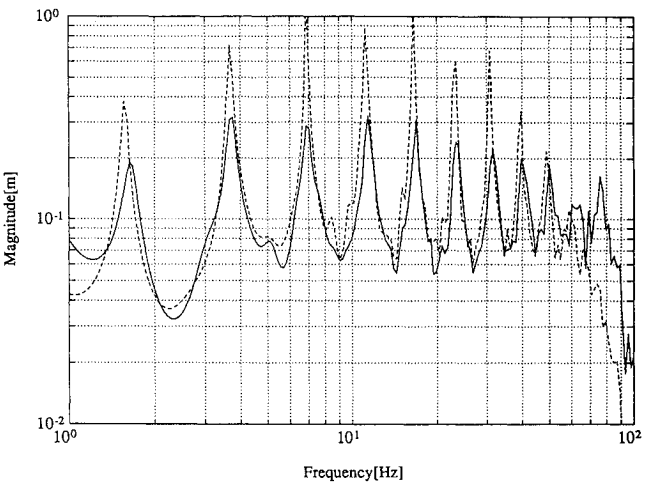


**Fig. 9 Measured open- (broken) and closed-loop (solid) transfer functions ($M_s/F$) using the compensator $C_2(s)$.**

Hz. At the high-frequency range the vibration modes are not well excited due to the unmodeled shaker's dynamics, and the signal-to-noise ratio is seen to be poor. Figure 8 shows the comparison between the magnitudes of the measured and designed compensators. As shown in Fig. 8 the compensator is not well implemented in the high-frequency range.

In the following experiments using the noncollocated sensor and actuator, the second-order low-pass filter is added, with poles at 300 Hz. A significant vibration peak, not instability, is notable at the high-frequency region without the low-pass filter since the position of the present sensor is at the node of the vibration mode of about 100 Hz. The vibration peak does not appear in the numerical simulation as shown in Figs. 3 and 4 because the sensor position is modeled as a discrete point, which has an infinitely small width in the numerical simulations, whereas that of the experiments has a finite width.

Figure 9 is shown to compare the measured transfer functions in the open loop and in the closed loop using the noncollocated $H_\infty$ compensator $C_2(s)$. Reasonable agreement is obtained between those results in Figs. 9 and 3. Some discrepancies are seen in the high-frequency region since the phase lag, about 30 deg at 100 Hz, is induced by the low-pass filter and the modeling error is dominated in the high-frequency range. Figure 10 shows that good agreement is obtained between the magnitudes of the measured and designed compensators.

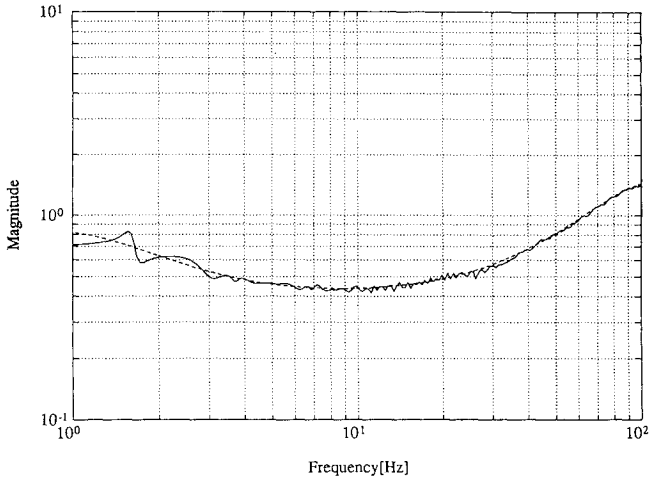


**Fig. 10 Desired (broken) and measured (solid) magnitudes of the compensator $C_2(s)$.**

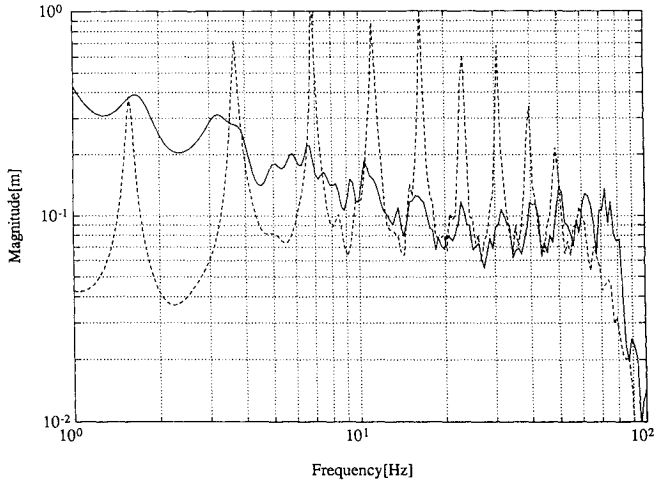


**Fig. 11 Measured open- (broken) and closed-loop (solid) transfer functions ($M_s/F$) using the compensator $C_3(s)$.**

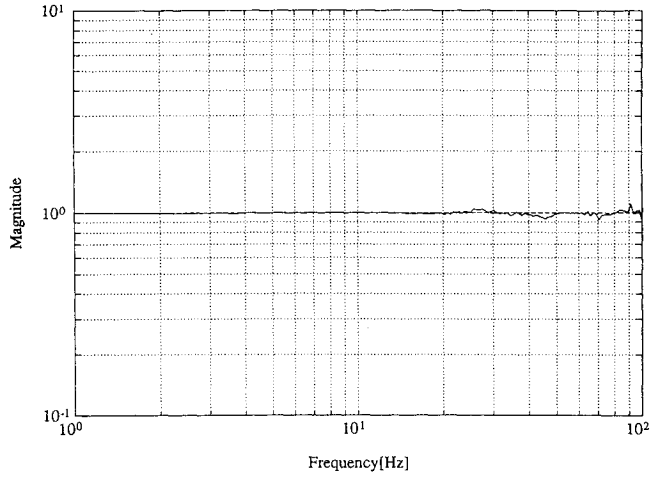


**Fig. 12 Desired (broken) and measured (solid) magnitudes of the compensator $C_3(s)$.**

Figure 11 compares the measured transfer functions in the open- and closed-loop cases using the compensator $C_3(s)$. Reasonable agreement is obtained between Figs. 11 and 4. Some discrepancies are seen due to the same reason as in the case of the compensator $C_2(s)$ in the high-frequency region. The measured damping amount is better than that calculated in the low-frequency region. This is because the response is constrained by the shaker so that it does not grow into large amplitude. Figure 12 shows that of the measured and desired compensators.

## IV. Conclusions

An approach for designing a broadband compensator is presented. This approach applies the $H_\infty$ control theory to the wave-absorbing control method and aims to minimize effects of the incoming waves on the outgoing waves at actuator positions in the sense that the $H_\infty$ norm of the closed-loop scattering matrix is minimum. The present approach for design guarantees a compensator to be a real causal function that can be rolled off in the high-frequency range if necessary. This approach can use various sensors that may be noncollocated at actuators and may be applied to a multi-input/multi-output system. The limitations are that the closed-loop system is not proved to be stable and that the method is not applicable to general structures that cannot be described by partial differential equations.

A vibration suppression control for a flexible beam is studied analytically and demonstrated experimentally as an application of the present approach. Compensators are designed for a collocated torque actuator and angle sensor and also for a noncollocated torque actuator and bending moment sensor. Performance of the compensator is analyzed in the frequency domain, and the broadband damping is achieved in both of these two cases. The measured open- and closed-loop transfer functions are obtained by using time histories of responses in random excitation tests. Good agreements are shown between the measured and calculated closed-loop transfer functions. Some discrepancies are seen due to the poor signal-to-noise ratio, the modeling error, and also the phase lag induced by the added low-pass filter in the cases of employing the collocated and noncollocated sensors, respectively. The large vibration is observed at about 100 Hz, at which the sensor position is the node of the vibration mode and is reduced through use of the low-pass filter. It is concluded that the designed compensators are able to attain sufficient broadband damping, and good agreement is shown between the experimental and simulated data for the frequency below 50 Hz.

## Appendix: Continued-Fraction Expansion for Rational Polynomial Approximation

Suppose that a set of $x_k$, $k = 0, 1, 2, \ldots$, is given. A continued-fraction expansion for a function $f(x)$ is

$$f(x) = \alpha_0 + \cfrac{x - x_0}{\alpha_1 + \cfrac{x - x_1}{\alpha_2 + \cfrac{x - x_2}{\alpha_3 + \cdots}}} \tag{A1}$$

where $\alpha_k = v_k(x_k)$ and $v_k(x)$ is defined by

$$v_0(x) = f(x), \qquad v_{k+1}(x) = (x - x_k)/\left[v_k(x) - v_k(x_k)\right] \qquad (k = 0, 1, 2, \ldots) \tag{A2}$$

A rational approximation $f_n(x)$ to the function $f(x)$ is obtained by truncating the continued fraction, Eq. (A1), after the $n$th term. The rational polynomial $f_n(x)$ is proper or improper depending on whether $n$ is even or odd. Note that $f_n(x_k) = f(x_k)$, $k = 1, 2, \ldots, n$, is always satisfied. A minimum value $x_0$ of the set of $x_k$, $k = 0, 1, 2, \ldots, n$, with equal logarithmic spacing, and a truncation number $n$ are adequately selected as $f_n(x)$ matches $f(x)$ well over the frequency range of interest in the compensator design and approximation.

## Acknowledgments

The authors would like to thank T. Ohtsuka and H. Okubo for their valuable comments and kind advice. They are grateful to Associate Editor S. M. Joshi and two anonymous reviewers for their helpful suggestions to the manuscript. The first author gratefully acknowledges the financial assistance of his parents during this research.

## References

[1]von Flotow, A. H., "The Acoustic Limit of Structural Dynamics," *Large Space Structures: Dynamics and Control,* edited by S. N. Atruli and A. K. Amos, Springer-Verlag, Berlin, 1988, pp. 213–238.

[2]Vaughan, D. R., "Application of Distributed Parameter Concepts to Dynamical Analysis and Control of Bending Vibrations," *Journal of Basic Engineering,* June 1968, pp. 157–166.

[3]von Flotow, A. H., and Schäfer, B., "Wave-Absorbing Controllers for a Flexible Beam," *Journal of Guidance, Control, and Dynamics,* Vol. 9, No. 6, 1986, pp. 673–680.

[4]Miller, D. W., Hall, S. R., and von Flotow, A. H., "Optimal Control of Power Flow at Structural Junctions," *Journal of Sound and Vibration,* Vol. 140, No. 3, 1990, pp. 475–497.

[5]Miller, D. W., and Hall, S. R., "Experimental Results Using Active Control of Travelling Wave Power Flow," *Journal of Guidance, Control, and Dynamics,* Vol. 14, No. 2, 1991, pp. 350–359.

[6]Mace, B. R., "Active Control of Flexural Vibrations," *Journal of Sound and Vibration,* Vol. 114, No. 2, 1987, pp. 253–270.

[7]Fujii, H., Ohtsuka, T., and Murayama, T., "Wave-Absorbing Control for Flexible Structures with Non-Collocated Sensors and Actuators," *Journal of Guidance, Control, and Dynamics,* Vol. 15, No. 2, 1992, pp. 431–439.

[8]Fujii, H., and Ohtsuka, T., "Experiment of a Noncollocated Controller for Wave Cancellation," *Journal of Guidance, Control, and Dynamics,* Vol. 15, No. 3, 1992, pp. 741–745.

[9]MacMartin, D. G., and Hall, S. R., "An $H_\infty$ Power Flow Approach to Control of Uncertain Structures," Massachusetts Inst. of Technology, SERC 4-90, Cambridge, MA, June 1990.

[10]MacMartin, D. G., and Hall, S. R., "Control of Uncertain Structures Using an $H_\infty$ Power Flow Approach," *Journal of Guidance, Control, and Dynamics,* Vol. 14, No. 3, 1991, pp. 521–530.

[11]Francis, B. A., *A Course in $H_\infty$ Control Theory,* Springer-Verlag, New York, 1987.

[12]Glover, K, Limebeer, D. J. N., Doyle, J. C., Kasenally, E. M., and Safonov, M. G., "A Characterization of All Solutions to the Four Block General Distance Problem," *SIAM Journal of Control and Optimization,* Vol. 29, No. 2, 1991, pp. 283–324.

[13]Chang, B. C., Li, X. P., Banda, S. S., and Yeh, H. H., "Robust Control System Design by $H_\infty$ Optimization Theory," *Proceedings of the AIAA Guidance, Navigation, and Control Conference* (New Orleans, LA), AIAA, Washington, DC, Aug. 1991, pp. 723–729.

[14]Bennett, W. H., Blankenship, G. L., and Kwatny, H. G., "Spectral Factorization and Homogenization Methods for Modeling and Control of Flexible Structures," Systems Engineering, Inc., SEI TR-86-14, Greenbelt, MD, 1986.